Single-Switch Voltage Equalizer Using Multi-Stacked Buck-Boost Converters for Partially-Shaded Photovoltaic Modules

Masatoshi Uno, *Member, IEEE*, and Akio Kukita

Abstract— **Partial shading on a photovoltaic (PV) string comprising multiple modules/substrings triggers issues such as a significant reduction in power generation and the occurrence of multiple maximum power points (MPPs), including a global and local MPPs, that encumber MPP tracking algorithms. Single-switch voltage equalizers using multi-stacked buck-boost converters are proposed to settle the partial shading issues. The single-switch topology can considerably simplify the circuitry compared with conventional equalizers requiring multiple switches in proportion to the number of PV modules/substrings. The proposed voltage equalizers can be derived by stacking capacitor-inductor-diode (CLD) filters on traditional buck-boost converters, such as SEPIC, Zeta, and Ćuk converters. The optimum equalization strategy is also proposed and discussed for the equalizers to compensate the partially-shaded PV modules efficiently. Operational analysis based on a simplified equivalent circuit is performed for a SEPIC-based topology. Experimental equalization tests using the SEPIC-based voltage equalizer were performed emulating partially-shaded conditions for a PV panel comprising of three substrings. Local MPPs were eliminated and extractable maximum powers increased by the equalizer, demonstrating the efficacy of the proposed voltage equalizer.**

Index Terms—**Buck-boost converter, partial shading, photovoltaic system, SEPIC, voltage equalizer.**

I. INTRODUCTION

To extract as much energy as possible from photovoltaic (PV) modules, the energy utilization needs to be improved, as well as power conversion efficiency of converters. Partial shading on a PV string comprising multiple modules/substrings (hereafter referred to as 'substring' unless otherwise noted) is known as a serious cause that significantly decreases energy utilization. In general, substring currents are dependent on irradiance, and shaded substrings are less capable of generating current than unshaded ones. If shaded substrings are no longer capable of a string current, bypass diodes connected in parallel start con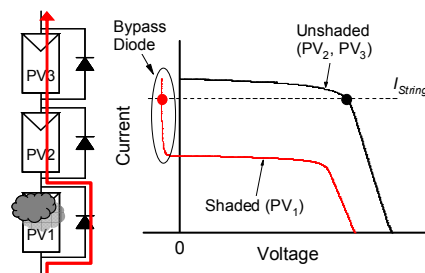ducting to bypass the shaded substrings, as shown in Fig. 1(a), resulting in a significant mismatch in operational voltage. This mismatch triggers multiple maximum power points (MPPs), including a global and local MPPs, as shown in Fig. 1(b), that encumber MPP tracking (MPPT) algorithms to track the global MPP (point A in Fig. 1(b)). In addition, even though the string as a whole is operated at a global MPP, some substrings in the string can never be fully utilized because of the operational voltage mismatch, significantly reducing the maximum extractable power.

Decentralized PV systems employing micro-inverters/converters for each individual PV module/substring to adopt distributed MPPT (DMPPT) are the most typical solution to these partial-shading issues, and their energy yield benefit for PV installation sites exploiting DMPPT has been investigated and demonstrated [1]. All PV modules/substrings are basically able to operate at each MPP, even under partial-shading conditions, due to the individual control for each module unless micro-converters operate outside a designed allowable range in terms of component
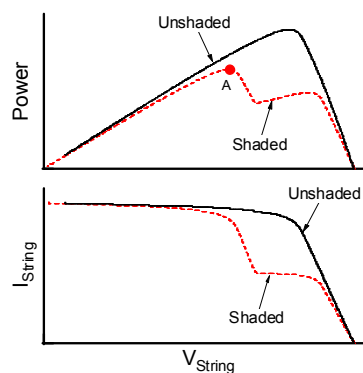
The authors are with Japan Aerospace Exploration Agency, Ibaraki 305-8505, Japan (e-mail: uno.masatoshi@jaxa.jp; kukita.akio@ jaxa.jp).
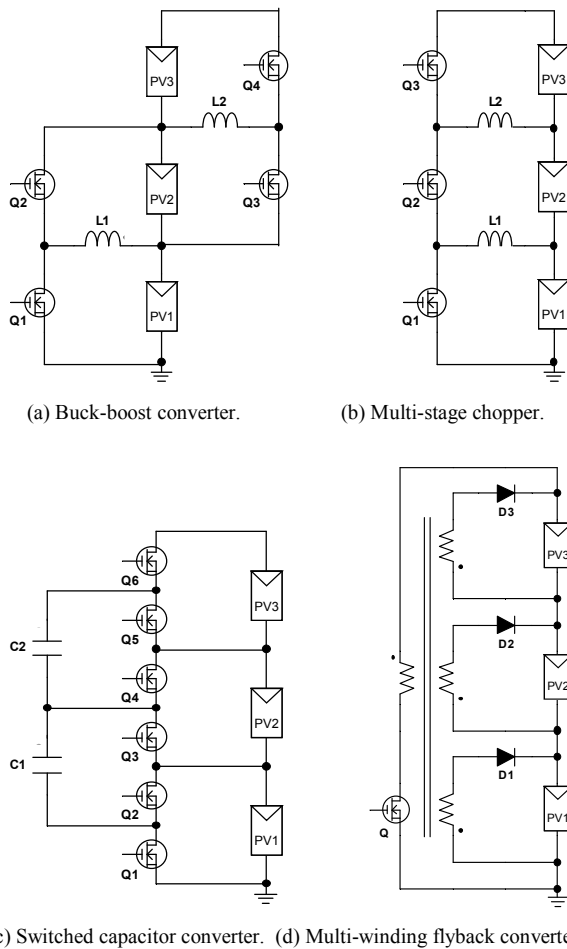

(a) Bypassed substring and its characteristic.

(b) String characteristics.

Fig. 1. PV string under partial shading condition: (a) bypassed substring and its characteristic, (b) string characteristics.

(a) Buck-boost converter.   (b) Multi-stage chopper.

(c) Switched capacitor converter. (d) Multi-winding flyback converter.
Fig. 2. Conventional DPP converters and voltage equalizers based on (a) buck-boost converter, (b) multi-stage chopper, (c) switched capacitor converter, and (d) multi-winding flyback converter.

ranting and duty cycle [1]–[4]. However, since the number of micro-inverters/converters is proportional to that of PV modules/substrings, systems tend to be complex and costly with increasing number of modules.

Differential power processing (DPP) converters and voltage equalizers are alternative powerful solutions to partial-shading issues. With DPP converters or equalizers, a fraction of the generated power of unshaded substrings is transferred to shade ones so that all the substrings operate at the same voltage or even at each MPP. Various kinds of DPP converters and equalizers have been proposed and developed [5]–[25], the representative topologies of which are listed in Fig. 2. These topologies are basically identical to cell voltage equalizers used for series-connected batteries/supercapacitors (SCs); equalizers based on buck-boost converters [26], multi-stage choppers [27], [28], switched capacitor converters [29]–[32], multi-winding forward/flyback converters [33]–[35], etc. [36], [37] have been proposed for battery/SC equalization.

In general, a switch count in a converter can be a good index to represent the circuit complexity, because each switch requires a gate driver circuit comprising a driver IC, auxiliary power source, and ancillary components. In most conventional

topologies, which are based on bidirectional converters shown in Figs. 2(a)–(c), such as buck-boost converters [5]–[12], multi-stage choppers [16], [17], switched capacitor converters [18], [19], and other topologies [13]–[15], [20]–[23], more than one switch per substring is required as a minimum, meaning the switch count tends to soar with increasing the number of substrings/modules. With the multi-winding flyback converter [25] shown in Fig. 2(d), the switch count can be reduced to one, simplifying the circuitry. However, the requirement for strict parameter matching among multiple secondary windings would be a design hurdle [36], [37], likely imposing a significant constraint.

In this paper, single-switch voltage equalizers using multi-stacked buck-boost converters are proposed. The proposed equalizers can be derived by stacking multiple capacitor-inductor-diode (CLD) filters on traditional buck-boost converters using two inductors, such as SEPIC, Zeta, and Ćuk converters. Regardless of the number of substrings/modules, the required switch count is only one, considerably simplifying the circuitry compared with conventional DPP converters and voltage equalizers. The optimum equalization strategy is first discussed in Section II based on a schematic diagram of the proposed voltage equalizers. Three representative topologies of the proposed voltage equalizers are shown in Section III, followed by operational analyses for the SEPIC-based voltage equalizer in Section IV. Section V introduces a control circuit to substantiate the optimum equalization strategy. The experimental results of the equalization tests emulating partially-shaded conditions performed for three PV substrings are shown in Section VI.

II. EQUALIZATION STRATEGY

A. General Description of the Proposed Voltage Equalizer

A schematic of the proposed single-switch voltage equalizer for a string comprising three substrings of PV_1–PV_3 with an MPPT converter is shown in Fig. 3. The string is connected to the input of the voltage equalizer and supplies the input current of $I_{eq\text{-}in}$. Meanwhile, the power supplied is redistributed to each substring as the equalization current $I_{eq\text{-}i}$ ($i = 1\ldots3$), depending on shading conditions. In other words, a fraction of the
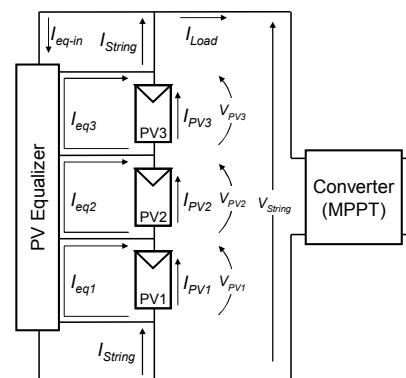

Fig. 3. Schematic of PV string with proposed voltage equalizer and MPPT converter.

generated power of the string is circulated through the voltage equalizer. In the course of power circulation, all substring voltages are equalized by preferentially redistributing power for shaded substrings, as explained in detail later.

The string current I_{String} is expressed as

$$I_{String} = I_{Load} + I_{eq-in} = I_{PVi} + I_{eq-i}, \tag{1}$$

where I_{Load} is the load current or the input current of the MPPT converter, I_{PVi} is the generated current of PV_i. Part of I_{String} is consumed as I_{eq-in} and then converted and redistributed to each substring as I_{eq-i}. Similar to conventional voltage equalizers, the proposed voltage equalizer operates so that all substring voltages become uniform. Accordingly, the shaded substrings in the string preferentially receive equalization currents from the equalizer because they are less capable of generating current of I_{PVi} and their voltages tend to be lower than those of unshaded substrings, as shown in Fig. 1. Meanwhile, the MPPT converter tracks the MPP of the string as a whole, similar to ordinary ones. In other words, the equalizer and MPPT converter independently operate.

B. Equalization Scenarios

There are three conceivable equalization scenarios: insufficient equalization, over-equalization, and optimum equalization. The operation points of each PV substring under a partially-shaded condition, where PV_1 and PV_2 are severely and moderately shaded, respectively, under the three equalization scenarios are shown in Fig. 4. As will be explained in the next section, the proposed voltage equalizer is basically a unidirectional converter that can produce uniform multiple output voltages. For the sake of simplicity, the voltage equalizer in Fig. 4 is equivalently illustrated as a multi-output voltage source producing uniform output voltage of V_e with ideal diodes.

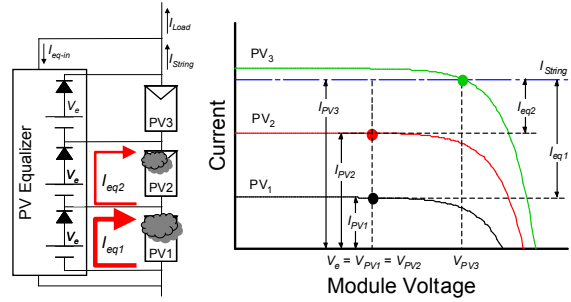*i) Insufficient equalization* ($V_{PV1} = V_e < V_{PV2} < V_{PV3}$ or $V_{PV1} = V_{PV2} = V_e < V_{PV3}$):

If the power supplied for the shaded substrings is insufficient to equalize all substring voltages, the operation is subject to insufficient equalization. The insufficient equalization for the example partially-shaded condition can be subdivided into Cases 1 and 2, according to the voltage relationship between V_e and $V_{PV1}-V_{PV3}$.

In Case 1 ($V_e = V_{PV1} < V_{PV2} < V_{PV3}$) shown in Fig. 4(a), PV_2 and PV_3 receive no current from the equalizer, their currents are equal to I_{String}, and they operate at respective voltage levels, which exceed V_{PV1}. Meanwhile, the equalizer supplies an equalization current of I_{eq1} for the severely-shaded substring of PV_1, but the power supplied for PV_1 is insufficient to boost V_{PV1} to other substring voltage levels. As shown in Fig. 4(a), the difference between I_{String} and generated current of PV_1 (i.e. I_{PV1}) corresponds to I_{eq1}, as expressed by (1). Since individual PV substring operate at totally different voltage levels, the overall string operates in a voltage-mismatched condition and partial shading issues would remain.
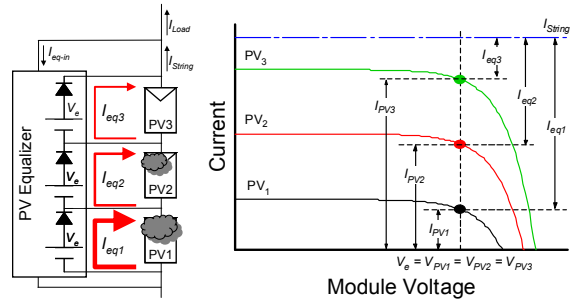
In Case 2 ($V_e = V_{PV1} = V_{PV2} < V_{PV3}$) shown in Fig. 4(b), the equalizer is more capable of supplying power for shaded
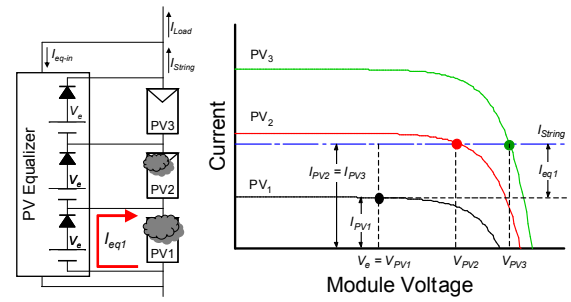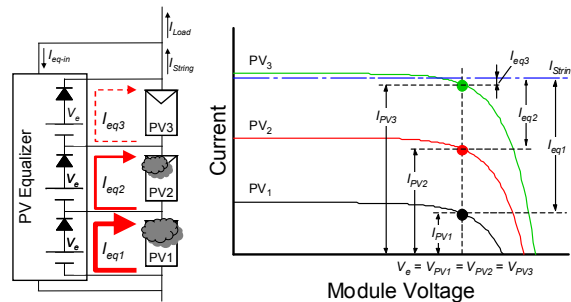

(a) Insufficient equalization Case 1.

(b) Insufficient equalization Case 2.

(c) Over-equalization.

(d) Optimum equalization.

Fig. 4. Operations under (a) insufficient equalization Case 1, (b) insufficient equalization Case 2, (c) over-equalization, and (d) optimum equalization.

substrings than in Case 1, but remains insufficient to equalize all voltages. The equalizer supplies currents for both the shaded substrings of PV_1 and PV_2; hence V_{PV1} and V_{PV2} are equal. However, the power supplied for PV_1 and PV_2 remains insufficient for their voltages of V_{PV1} and V_{PV2} to reach V_{PV3}, resulting in a voltage mismatch as $V_e = V_{PV1} = V_{PV2} < V_{PV3}$.

ii) Over-equalization ($V_e = V_{PV1} = V_{PV2} = V_{PV3}$):

In this scenario, the voltage equalizer supplies equalization currents for not only the shaded substrings but also those unshaded, so that all substring voltages are equalized as $V_e =$

$V_{PV1} = V_{PV2} = V_{PV3}$, as shown in Fig. 4(c). With the support of the voltage equalizer, all the substrings virtually exhibit equivalent characteristics when illustrated in I_{String} vs. V_{PVi} characteristics, and therefore, partial-shading issues would be precluded.

The apparent I_{String} is rather larger than even the unshaded substring's current of I_{PV3}, indicating that the unshaded substring of PV$_3$ needlessly receives the relatively large equalization current of I_{eq3}; I_{String} is the sum of I_{PVi} and I_{eq-i}. A fraction of I_{String} is used as I_{eq-in} that is then converted and redistributed to each substring as I_{eq1}–I_{eq3}. As expressed by (1), the larger value of I_{eq-in} or I_{eq-i} under the over-equalization scenario, the larger the value of I_{String} will be, needlessly increasing processed power as well as power conversion loss in the voltage equalizer. Therefore, to eliminate unnecessary power conversion loss in the equalizer, equalization should be performed such as to minimize the unnecessary equalization current for the unshaded substring.

iii) Optimum equalization ($V_e = V_{PV1} = V_{PV2} = V_{PV3}$):

This scenario equates to the boundary between over-equalization and the insufficient equalization in Case 2. Both the voltage relationship and the current paths are similar to those under the over-equalization scenario; the equalizer supplies equalization currents for all substrings, including unshaded, so that all substring voltages are equalized as $V_e = V_{PV1} = V_{PV2} = V_{PV3}$. The difference from the over-equalization scenario is that the current supplied for the unshaded substring of PV$_3$, I_{eq3}, is minimized to nearly zero, as shown in Fig. 4(d), to reduce processed power as well as power conversion loss in the equalizer. As can be compared with Fig. 4(c), minimizing I_{eq3} also reduces I_{eq1} and I_{eq2}, while the operational substring voltages are identical to those under the over-equalization. To materialize this optimum equalization strategy, currents supplied to unshaded substrings need to be controlled. A control circuit to substantiate this optimum equalization strategy will be introduced in Section V.

III. SINGLE-SWITCH VOLTAGE EQUALIZER USING MULTI-STACKED BUCK-BOOST CONVERTERS

The topologies of the proposed voltage equalizers basically

(a) SEPIC.

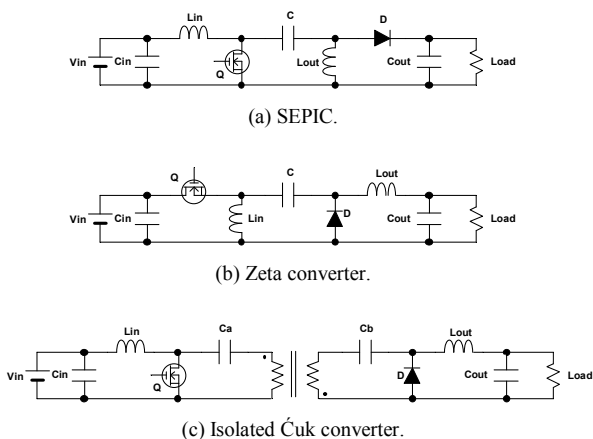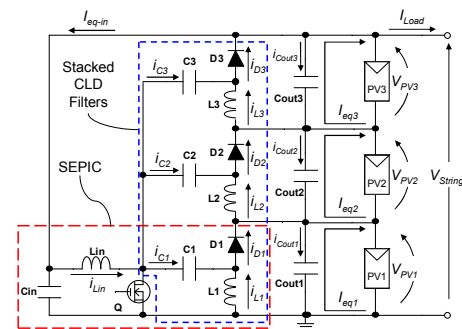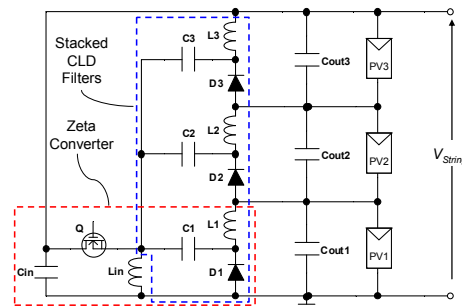(b) Zeta converter.

(c) Isolated Ćuk converter.

Fig. 5. Buck-boost converters usable as a foundation for the proposed equalizers.

resemble those developed for series-connected energy storage cells, such as SCs and lithium-ion batteries [38]. Proposed single-switch voltage equalizers can therefore be derived based on traditional buck-boost converters using two inductors, such as SEPIC, Zeta, Ćuk converters, as listed in Fig. 5. A non-isolated Ćuk converter cannot be used as a basic circuit due to its inverting voltage conversion property.

The proposed single-switch voltage equalizers for three PV substrings are shown in Fig. 6. Each PV equalizer is based on one of the buck-boost converters with stacked CLD filters. In all proposed equalizer topologies, an asymmetric square-wave voltage is produced across the switch Q (as will be shown in Figs. 8 and 10), and capacitors C$_1$–C$_3$ act as coupling capacitors, allowing only the ac component to flow through. Although the stacked CLD filters have different dc voltage levels, the same asymmetric square voltage wave is applied to all inductors L$_1$–L$_3$ due to the ac coupling, producing a uniform output voltage for each PV substring.

(a) SEPIC-based.

(b) Zeta-based.
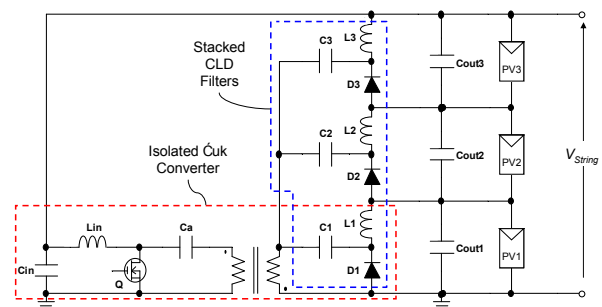
(c) Ćuk-based.

Fig. 6. Proposed single-switch voltage equalizer using multi-stacked buck-boost converters for partially-shaded series-connected PV modules.

As mentioned in Section I, the switch count is a good index to represents the circuit complexity. There is only one switch in each topology, dramatically simplifying the circuitry compared with conventional DPP converters and voltage equalizers, shown in Figs. 2(a)–(c), that require numerous switches proportional to the number of substrings/modules. Although the proposed equalizers are advantageous in terms of switch count, it should be noted as a drawback that the proposed equalizers require a current sensor for each substring to realize the optimum equalization, as will be discussed in Section V. Among the proposed voltage equalizers shown in Fig. 5, the SEPIC-based topology is considered the most promising due to the lack of a floating-gate driver and transformer; a floating-gate driver is necessary for the Zeta-based equalizer, and the Ćuk-based topology is unfeasible without the transformer.

Although equalizers shown in Fig. 6 are for a panel consisting of three substrings, the propose voltage equalizers can be applied to any number of substrings/modules; the equalizers can be extended by increasing the number of stacked CLD filters and adjusting component rating, as will be discussed in Section IV-D. The proposed equalizers can naturally be applied to either substrings or modules. However, since each substring/module needs to be wired to the equalizer, extending to a large string consisting of numerous substrings/modules will be cumbersome in terms of wiring. Meanwhile, increased component rating will also be of concern for a high-voltage string, as will be discussed in Section IV-D.

DPP converters based on buck-boost converters or multi-stage choppers, shown in Figs. 2(a) and (b), respectively, allow all substrings to operate at their MPP, even under partially-shaded conditions, by individually controlling duty cycles [7], [8], [16] and [17]. This individual MPPT can maximize solar energy utilization. However, since the duty cycles for each converter must be properly determined depending on partial-shading conditions, control tends to be complex and communication devices between adjacent converters are necessary. On the other hand, there is only one switch to be controlled in the proposed equalizer, allowing a relatively simple control. However, similar to conventional voltage equalizers based on switched capacitor converters [18], [19], the proposed voltage equalizers operate so that voltages of substrings are simply equalized—the concept of the voltage equalization itself is not novel—, and hence, the individual MPPT is unfeasible with the proposed equalizer. Since substring voltages cannot be individually controlled, energy utilization with the proposed voltage equalizer under partially-shaded conditions would be inferior to that with DPP converters using buck-boost converters or multi-stage choppers. However, equalizing voltages simply would be effective enough for substrings to operate at each near-MPP when consider the fact that MPP voltages are relatively insensitive to shading conditions compared to currents [18], [22], [23].

IV. OPERATION ANALYSIS

The proposed voltage equalizers operate either in continuous conduction mode (CCM) or discontinuous conduction mode (DCM), similar to traditional buck-boost converters [39], [40]. In the previous work for battery/SC equalization, voltage equalizers were designed to operate in DCM, in which currents in equalizers can be automatically limited to within desired levels, even without feedback control, to eliminate the feedback control loop [38]. In the proposed voltage equalizers for PV modules, conversely, the equalizers are controlled to realize the optimum equalization strategy, as discussed in Section II-B. This means the open-loop operation in DCM is no longer advantageous, and the CCM operation is considered desirable from the perspective of current rating of components. However, similar to ordinary switching converters operating under light-load conditions, DCM operation is likely when the degree of shading is light; slightly-shaded conditions are equivalent to light-load conditions for ordinary converters.

The fundamental operation of the proposed equalizer is somewhat similar to that of the battery/SC equalizer [38]. However, operational analysis of the proposed equalizer shown in Fig. 6(a) would be cumbersome because each CLD filter has a different dc current level depending on the degree of shading. In addition, equations developed in [38] cannot directly be applied to the proposed equalizer, unless the circuit is modified. In this subsection, a simplified equivalent circuit is derived to facilitate the operational analysis; operation modes are explained using the original circuit shown Fig. 6(a), while mathematical analyses will be performed for the simplified circuit, with which equations developed in [38] can be applied. For convenience, the DCM operation is initially explained based on [38] and [41], followed by the CCM operational analysis.

A. Simplified Equivalent Circuit

Based on Kirchhoff's current law in Fig. 6, the average current of L_i, I_{Li}, equates to that of D_i, I_{Di}, because the average current of C_i must be zero under a steady-state condition. Comparing Figs. 3 and 6, the equalization current supplied to PV_i, I_{eq-i} is

$$I_{eq-i} = I_{Li} = I_{Di}. \tag{2}$$

Therefore, both I_{L1}–I_{L3} and I_{D1}–I_{D3} are dependent on partial-shading conditions.

As mentioned in Section III, thanks to the ac coupling of C_1–C_3, all inductors of L_1–L_3 are driven by the same asymmetric square-wave voltage, although the stacked CLD filters are at different dc voltage levels. Since the stacked CLD filters are ac-coupled, the series-connected substrings can be equivalently separated and grounded as shown in Fig. 7(a), in which a dc voltage source with V_{String} that is equivalent to the sum of V_{PV1}–V_{PV3} is used to power the equalizer. In this transformed voltage equalizer, both the CLD filters and PV_1–PV_3 are connected in parallel. Accordingly, the transformed circuit shown in Fig. 7(a) can be simplified to the equivalent circuit shown in Fig. 7(b), which is identical to a traditional SEPIC shown in Fig. 5(a). This allows the overall operation of the proposed voltage equalizer to be analyzed and expressed

(a) Transformed circuit.
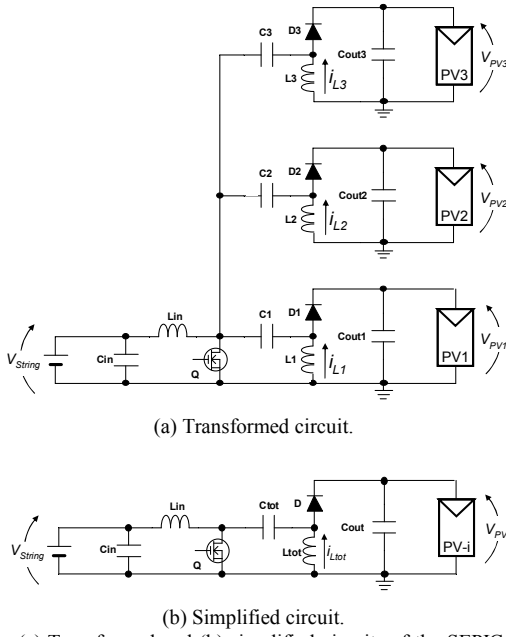

(b) Simplified circuit.

Fig. 7. (a) Transformed and (b) simplified circuits of the SEPIC-based voltage equalizer.

similarly to the traditional SEPIC.

This simplification is feasible because all substring voltages are basically rendered uniform provided the equalizer operates under the over- or optimum equalization scenarios explained in Section II-B. For battery/SC equalization, conversely, this simplification is unfeasible because batteries/SCs are voltage sources and their voltages are basically nonuniform when equalization is necessary.

In the simplified equivalent circuit, the current of L_{tot}, i_{Ltot}, equates to the sum of i_{L1}–i_{L3};

$$i_{Ltot} = i_{L1} + i_{L2} + i_{L3} . \qquad (3)$$

From (2) and (3), the total of I_{eq1}–I_{eq3}, $I_{eq\text{-}tot}$, is

$$I_{eq\text{-}tot} = I_{eq1} + I_{eq2} + I_{eq3} = I_{Ltot} . \qquad (4)$$

Since all inductors in the CLD filters are driven by the same asymmetric square-wave voltage of v_L, the inductance of L_{tot} in the simplified circuit, L_{tot}, is yielded as

$$L_{tot} = v_L \left(\frac{dt}{di_{L1}} + \frac{dt}{di_{L2}} + \frac{dt}{di_{L3}} \right) = \frac{L_i}{3} , \qquad (5)$$

where L_i is the inductance of L_1–L_3 in the original circuit shown in Fig. 6(a).

Capacitors C_1–C_3 and C_{out1}–C_{out3}, respectively, are virtually connected in parallel, and therefore, the capacitances of C_{tot} and C_{out} in the simplified circuit, C_{tot} and C_{out}, are

$$C_{tot} = 3C_i , \quad C_{out} = 3C_{out\text{-}i} , \qquad (6)$$

where C_i and $C_{out\text{-}i}$, respectively, are the capacitances of C_1–C_3 and C_{out1}–C_{out3} in the original circuit shown in Fig. 6(a).

B. DCM Operation

As explained in Section II-B, the proposed voltage equalizer under the optimum equalization scenario supplies equalization currents for all substrings, including unshaded ones. The key operation waveforms and current flow paths in DCM under the

partially-shaded condition are shown in Figs. 8 and 9, respectively. It should be noted that Figs. 8 and 9 are illustrated assuming that currents from the equalizer to PV substrings are buffered by smoothing capacitors C_{out1}–C_{out3}; $I_{eq\text{-}in}$ and I_{eq1}–I_{eq3} are not depicted in Fig. 8 because they are basically dc thanks to C_{out1}–C_{out3}.

During the on period, T_{on}, all inductor currents, i_{Lin} and i_{Li}, linearly increase and flow through the switch Q. i_{L1}–i_{L3} flow through C_1–C_3 and C_{out1}–C_{out2}. The lower the position of C_{out1}–C_{out3}, the higher the current tends to flow; the current of C_{out1}, i_{Cout1}, shows the largest amplitude. For example, i_{L2} only flows through C_{out1}, whereas i_{L3} flows through both C_{out1} and C_{out2}. Thus, currents flowing through the upper smoothing capacitors are superimposed on lower ones.

As Q is turned off, the operation moves to $T_{off\text{-}a}$ period. Diodes D_1–D_3 start conducting, and the inductor current linearly declines. Energies stored in L_1–L_3 in the previous T_{on} period are discharged to respective smoothing capacitors in this mode. i_{Lin} is distributed to C_1-D_1–C_3-D_3 branches and flows toward C_{out1}–C_{out3}. Depending on the shading conditions, some diodes that correspond to slightly-shaded or unshaded substrings cease to conduct sooner than the others. For example, i_{D3} reaches zero sooner than i_{D1} and i_{D2}, as can be seen in Fig. 8. After i_{D3} declines to zero, i_{L3} flows toward C_1 and C_2 through C_3. Until all diode currents decrease to zero, this $T_{off\text{-}a}$ period lasts and all inductor currents keep linearly decreasing. Similar to the T_{on} period, the higher current tends to flow through smoothing capacitors in the lower place due to the current superposition. Note that some inductor currents that correspond to slightly-shaded or unshaded substrings (i_{L3} in Fig. 8) become negative in this period (as well as in the next period), although arrows in Fig. 9 are depicted assuming the sign of i_{L3} is always positive.

The $T_{off\text{-}b}$ period begins as all diodes cease. Since the applied voltages of all inductors in this period are zero, all currents, including i_{Ci}, remain constant.
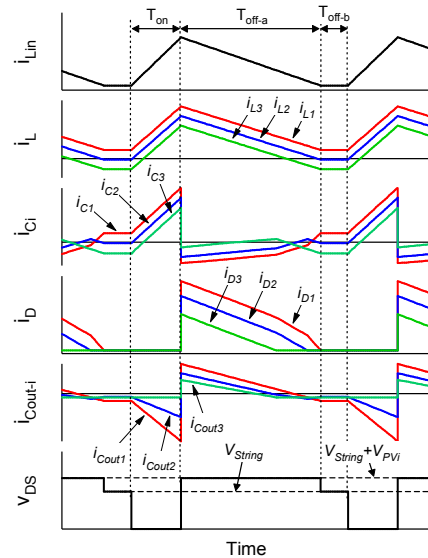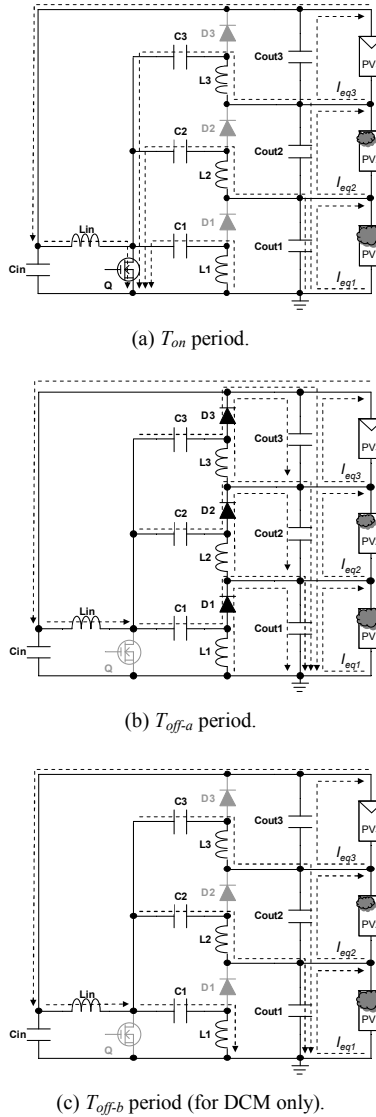

Fig. 8. Key operation waveforms in DCM.

(a) T_{on} period.

(b) T_{off-a} period.

(c) T_{off-b} period (for DCM only).

Fig. 9. Current flow paths in period of (a) T_{on}, (b) T_{off-a}, and (c) T_{off-b} (for DCM only).

From the previous work [38], the duty cycle of T_{off-a} period, D_a, is given by

$$D_a = \frac{D V_{String}}{V_{PVi} + V_D}, \tag{7}$$

where D is the duty cycle of Q, and V_D is the forward voltage drop of the diodes. The average currents of L_{tot} and L_{in}, I_{Ltot} and I_{Lin}, are expressed as

$$I_{Ltot} = \frac{V_{String} D D_a T_S}{2}\left(\frac{L_{in} + L_{tot}}{L_{in} L_{tot}}\right), \tag{8}$$

$$I_{Lin} = \frac{V_{String} D^2 T_S}{2}\left(\frac{L_{in} + L_{tot}}{L_{in} L_{tot}}\right), \tag{9}$$

where T_S is the switching period, L_i and L_{in} are the inductances of L_i and L_{in}, respectively. From (8) and (9),

$$\frac{I_{Ltot}}{I_{Lin}} = \frac{D_a}{D}, \tag{10}$$

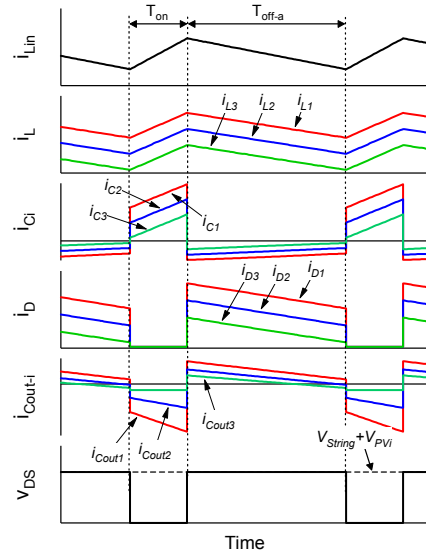According to (4) and (8), D and D_a increase with the demand

Fig. 10. Key operation waveforms in CCM.

for $I_{eq-tot} (= I_{Ltot})$. If $D_a > 1 - D$, the equalizer operates in CCM. The boundary between DCM and CCM is established based on the critical duty cycle, $D_{critical}$;

$$D_{critical} = \frac{V_{PVi} + V_D}{V_{String} + V_{PVi} + V_D}. \tag{11}$$

C. CCM Operation

The operational waveforms in CCM are shown in Fig. 10. The current flow paths in CCM are similar to those in DCM in T_{on} and T_{off-a}, shown in Figs. 9(a) and (b), respectively.

Similar to the traditional SEPIC, the voltage conversion ratio and current relationship in CCM are given by

$$V_{PVi} = \frac{D}{1-D} V_{String} - V_D, \tag{12}$$

$$\frac{I_{Ltot}}{I_{Lin}} = \frac{1-D}{D}. \tag{13}$$

D. Component Rating

i) Inductors:

Similar to ordinary converters, inductance values of L_i and L_{in} should be designed considering a full load condition. The full load condition occurs when one substring in unshaded while the rest two substrings are completely shaded; each shaded substring produces no power but requires as much power as the unshaded one produces. Thus, in terms of a processed power, the full load condition is considered as the worst shading condition. Ripple ratios of I_{Li} and I_{Lin}, α_{Li} and α_{Lin}, are defined as

$$\begin{cases} \alpha_{Li} = \dfrac{\Delta I_{Li}}{I_{Li}} = \dfrac{V_{String} D T_S}{L_i I_{eq-i}} \\[2mm] \alpha_{Lin} = \dfrac{\Delta I_{Lin}}{I_{Lin}} = \dfrac{V_{String}(1-D) T_S}{L_{in} I_{eq-tot}} \end{cases}, \tag{14}$$

where ΔI_{Li} and ΔI_{Lin} are the ripple currents of L_i and L_{in}. Although these values vary depending on shading conditions, $\alpha_{Li} = \alpha_{Lin}$ for the worst shading case is deemed a reasonable

design. The worst shading condition occurs when two substrings are fully shaded, and therefore, $I_{eq\text{-}tot} = 2I_{eq\text{-}i}$. If $V_{PVi} \gg V_D$, (12) and (14) yield

$$\frac{L_i}{L_{in}} = \frac{D}{1-D}\frac{I_{eq\text{-}tot}}{I_{eq\text{-}i}} \approx \frac{2}{3} . \tag{15}$$

ii) Capacitors (C_1–C_3):

Since the substring voltages are equalized as $V_{PVi} = V_{String}/3$, the voltages of C_1–C_3, V_{C1}–V_{C3}, are

$$V_{C1} = V_{String}, \; V_{C2} = \frac{2}{3}V_{String}, \; V_{C3} = \frac{1}{3}V_{String} . \tag{16}$$

Since V_{String} is the sum of substring voltages, (16) indicates a tendency that the larger the number of substrings in a string, the higher voltage rating will be necessary for capacitors.

Assuming that the inductor current is ideally constant as I_{Li} with no ripple, the current of C_i, i_{Ci}, is expressed as

$$i_{Ci} = \begin{cases} I_{Li} & : T_{on} \\ \dfrac{D}{1-D}I_{Li} & : T_{off\text{-}a} \end{cases} . \tag{17}$$

The RMS current of C_i, $I_{RMS\text{-}Ci}$, is

$$I_{RMS\text{-}Ci} = I_{Li}\sqrt{\frac{D}{1-D}} . \tag{18}$$

iii) Smoothing Capacitors (C_{out1}–C_{out3}):

The RMS current rating of $C_{out\text{-}i}$ needs to be determined considering each capacitor position because of the current superposition, as mentioned in Section IV-B and shown in Fig. 9. Currents from the stacked CLD filters are buffered by $C_{out\text{-}i}$, while $C_{out\text{-}i}$ supplies an equalization current of $I_{eq\text{-}i}$ for PV_i. From (2) and (17) with the current flow paths shown in Figs. 9(a) and (b), the current of C_{out1}, i_{Cout1}, is expressed as

$$i_{Cout1} = \begin{cases} -(i_{C2}+i_{C3})-I_{Eq1} = -(I_{L1}+I_{L2}+I_{L3}) & : T_{on} \\ I_{L1}+(i_{C1}+i_{C2}+i_{C3})-I_{Eq1} = \dfrac{D}{1-D}(I_{L1}+I_{L2}+I_{L3}) & : T_{off\text{-}a} \end{cases} . \tag{19}$$

From (18) and (19), the RMS currents of C_{out1}, $I_{RMS\text{-}Cout1}$, is yielded as

$$I_{RMS\text{-}Cout1} = (I_{L1}+I_{L2}+I_{L3})\sqrt{\frac{D}{1-D}} = I_{RMS\text{-}C1} + I_{RMS\text{-}C2} + I_{RMS\text{-}C3} . \tag{20}$$

This equations confirms that the currents flowing from C_2 and C_3 are superimposed on C_{out1}, increasing the RMS current. Although $I_{RMS\text{-}Cout1}$ was yielded as an example, $I_{RMS\text{-}Cout2}$ and $I_{RMS\text{-}Cout3}$ can be obtained in the similar manner. Equation (20) implies that the RSM current of $C_{out\text{-}i}$ tends to increase with the number of substrings in a string, likely becoming a design limitation to scale up the string configuration.

iv) Switch and Diodes:

The voltage rating of the switch and diodes must be higher than their applied voltage during $T_{off\text{-}a}$ and T_{on} periods, respectively. The voltage across the switch in $T_{off\text{-}a}$ and diodes in T_{on}, V_{DS} and V_R, respectively, are the same as

$$V_{DS} = V_R = \frac{4}{3}V_{String}, \tag{21}$$

thus the required voltage rating of the switch and diodes increases with the number of substrings in a string because V_{String} is the sum of substring voltages. Note that V_R for each diode is independent on their positions.

From the current flow paths shown in Fig. 9(a), peak currents of the switch, $I_{Q\text{-}peak}$, is expressed as

$$I_{Q\text{-}peak} = I_{Lin} + \frac{\Delta I_{Lin}}{2} + I_{Ltot} + 3\frac{\Delta I_{Li}}{2} = \frac{I_{Ltot}}{1-D} + \frac{V_{String}DT_S}{2}\frac{L_{in}+L_{tot}}{L_{in}L_{tot}} \tag{22}$$

The average diode current in $T_{off\text{-}a}$ is given by $I_{Li}/(1-D)$, and therefore, the diode peak current, $I_{Di\text{-}peak}$, can be expressed as

$$I_{Di\text{-}peak} = \frac{1}{1-D}\left(I_{Li}+\frac{\Delta I_{Li}}{2}\right) = \frac{1}{1-D}\left(I_{Li}+\frac{V_{String}DT_S}{2L_i}\right) . \tag{23}$$

E. Impact of Component Tolerance

As all PV substrings are connected to respective CLD filters, the impact of component tolerance in CLD filters on voltage equalization performance should be considered.

As expressed by (7) and (12), V_{PVi} depends on D, D_a, and V_D, whereas neither is dependent on the capacitance of C_1–C_3 or the inductance of L_1–L_3, which implies that a mismatch in V_D could affect equalization performance. However, provided V_{PVi} is sufficiently higher than V_D, as in many PV applications, the mismatch in V_D would not have a significant impact.

Similar to the traditional SEPIC, C_1–C_3 in the proposed equalizer are coupling capacitors and designed to be sufficiently large so that their voltages can be regarded constant during operation. Therefore, provided they are large enough, the equalization performance is unaffected by capacitance mismatch.

Inductance mismatch also has no significant impact. Even if L_1–L_3 are not well-matched and the inclinations of i_{L1}–i_{L3} differ, V_{PV1}–V_{PV3} would be equalized. The simulation waveforms of the inductance-mismatched voltage equalizer operating in DCM where PV_1 and PV_2 are equally shaded are shown in Fig. 11; inductances are severely mismatched as L_2 is 70% of L_1 and L_3. The average currents of i_{L1} and i_{L2} are equal and independent of the inductance mismatch because they are simply dependent on their degree of shading, as (2) indicates. Conversely, as all inductors are driven by the same asymmetric square-wave voltage of v_L thanks to the ac coupling of C_1–C_3, as explained in
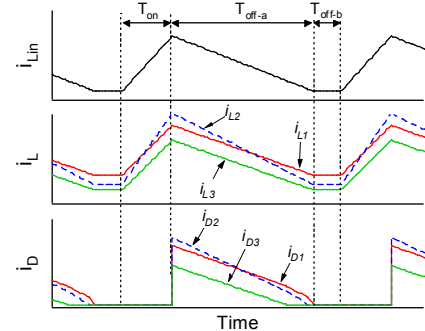

Fig. 11. Waveforms of inductance-mismatched equalizer operating in DCM.

Section IV-A, the inductance mismatch causes nonuniformity in di/dt. Although the inclinations of i_{L1}–i_{L3} differ, all of i_{L1}–i_{L3} linearly increase and decrease for the entire T_{on} and T_{off-a} periods, respectively (i_{L1}–i_{L3} in T_{off-a} period keep decreasing until all diodes cease, although D_3 ceases to conduct sooner). Thus, all of L_1–L_3 share the same values as D and D_a (or T_{on} and T_{off-a}), whereupon it emerges that V_{PV1}–V_{PV3} become uniform based on the volt-second balance on each inductor.

V. CONTROL CIRCUIT FOR OPTIMUM EQUALIZATION STRATEGY

As discussed in Section II-B, to materialize the optimum equalization strategy, equalization currents supplied to unshaded substrings need to be controlled, and this can be substantiated by either analog or digital feedback control. In this paper, an analog control circuit is employed.

An analog control circuit that substantiates the optimum equalization strategy is depicted in Fig. 12. This control circuit is similar to a typical PWM-control circuit, except for the minimum equalization current detector. Inductor average currents I_{L1}–I_{L3} measured with current sensors are used as I_{eq1}–I_{eq3} (see (2)), and the outputs of the current sensors' buffer amplifies (A_1–A_3) are connected to the error amplifier through respective diodes D_{a1}–D_{a3}. A diode corresponding to the minimum equalization current of I_{eq-min} conducts, whereas other diodes are reverse-biased. In the partial shading condition shown in Fig. 4(d), for example, PV$_3$ is unshaded and I_{eq3} is the smallest among I_{eq1}–I_{eq3}, and therefore, the output voltage level of A_3 is lower than the others. Accordingly, small current flows through D_{a3} from V_{CC} while D_{a1} and D_{a2} are reverse-biased. This means that I_{eq3} is inputted as I_{eq-min} to the inverting input of the error amplifier and is compared with the reference current of I_{ref}. The comparator compares the error amplifier's output voltage with the sawtooth carrier wave, producing a PWM signal. Thus, with this control circuit, the voltage equalizer operates so that I_{eq-min} equates to I_{ref}.

As discussed in Section II-B, optimum equalization can be realized when unshaded substrings receive equalization currents from the equalizer. To reduce the processed power as well as power conversion loss in the equalizer, equalization currents for unshaded substrings should be minimized; $I_{ref} = 0$ is ideal. However, since $I_{ref} = 0$ corresponds to the boundary between the optimum and insufficient equalization scenarios—some substring does not receive equalization current under insufficient equalization scenarios (i.e. $I_{eq-min} = 0$)—, I_{ref} should be set exceeding zero and be determined considering the accuracy of the current sensors so that the equalizer stably operates under the optimum equalization scenarios, regardless of noise. The value of I_{ref} was empirically determined as 50 mA in the experiments. It should be noted that equalization currents equal to I_{ref} always flow toward unshaded substrings under the optimum equalization scenario, regardless of whether substring characteristics are mismatched. In other words, if there is no partial shading and all the substring characteristics are matched, all the substrings receive an equalization current equal to I_{ref}.
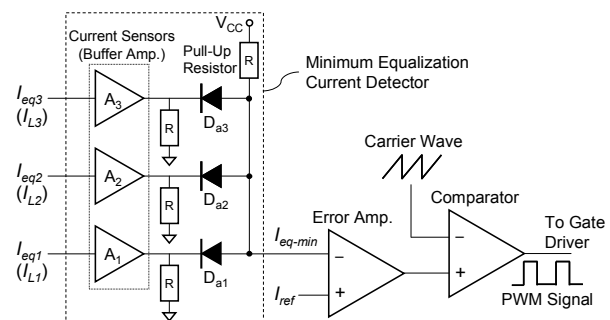
Fig. 12. Control circuit for optimum equalization.

Therefore, given that substring voltages are 12 V and an equalizer's light load efficiency is 80%, a processed power and power conversion loss in the equalizer will be 1.8 W (= 50 mA × 12 V × 3 substrings) and 0.45 W, respectively.

The proposed equalizer in practical use operates in concert with an MPPT converter as shown in Fig. 3; the equalizer precludes the negative impact of partial shading while the MPPT converter dynamically tracks the string's MPP by adjusting the current (i.e. I_{Load} in Fig. 3). In general, MPPT converters operate with sampling interval of longer than milliseconds. Meanwhile, the control circuit introduced in this section is basically similar to a typical feedback control loop, with which the equalizer's dynamic response is considered rather faster than that of MPPT converters. In other words, I_{Load} viewed from the equalizer can be regarded temporary fixed at a given time, and hence, the equalizer's operation is considered unaffected by the MPPT converter.

Obviously, the requirement for multiple current sensors is a major drawback of this control circuit and our future work will involve seeking alternative control circuits that do not rely on current sensors.

VI. EXPERIMENTAL RESULTS

A. Prototype and its Power Conversion Efficiency

A prototype was designed targeting a 100-W PV panel consisting of three 33-W substrings each with typical operating voltage range of 10–14 V (i.e. $V_{String} = 30$–42 V). A processed power in the equalizer becomes the largest when one substring is unshaded while the rest two substrings are completely shaded; each shaded substring produces no power and requires 33 W for
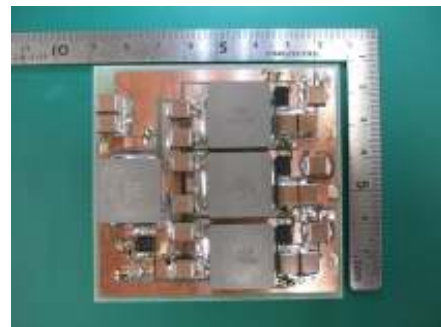
Fig. 13. A photograph of the 75-W prototype for three substrings in series.

Table I. Component values.

Component	Value
C_1–C_3	Ceramic Capacitor, 44 µF, 5 mΩ
C_{out1}–C_{out3}	Ceramic Capacitor, 141 µF
D_1–D_3	PDS4150, V_D = 0.71 V
L_{in}	82 µH, 87.3 mΩ
L_1–L_3	68 µH, 72.1 mΩ
Q	FDS86240, R_{DS} = 35.3 mΩ

equalization. The prototype was designed considering this worst condition in terms of processed power, although it is somewhat extreme and unrealistic. A photograph of a 75-W prototype of the proposed SEPIC-based voltage equalizer is shown in Fig. 13. The component values are listed in Table I. The inductance values (L_1–L_3 and L_{in}) and the switching frequency (170 kHz) were determined so that the volume of the prototype was reasonable and the values of α_{Li} and α_{Lin} (see (14)) were about 0.3 under the worst shading condition mentioned above.

The power conversion efficiencies of the prototype were measured using the experimental setup shown in Fig. 14(a), with which current flow paths under partially-shaded conditions can be emulated. It should be noted that 'efficiency' in this subsection refers to 'net power conversion efficiency' of the prototype without PV substrings. The voltage equalizer was powered by an external voltage source V_{ext} with 36 V that corresponds to V_{String} in a practical case. Meanwhile, PV substrings were removed and an electronic load operating in constant voltage mode was used. Selecting the intermediate tap of S_1 emulates a PV_1-shaded condition. When S_2 is selected, conversely, the shaded condition whereby PV_1 and PV_2 are
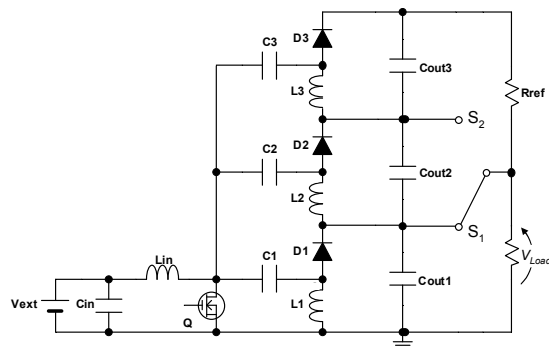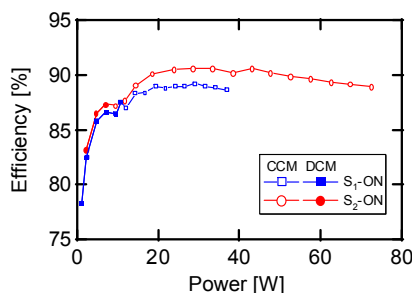
equally shaded can be emulated. The resistor R_{ref} was connected to provide the current path to draw equalization currents equal to I_{ref} = 50 mA from unshaded substrings. To emulate voltage-equalized conditions with I_{ref} = 50 mA, measurement was performed with V_{Load} = 12 V and R_{ref} = 480 Ω, and V_{Load} = 24 V and R_{ref} = 240 Ω when S_1 and S_2 were selected, respectively (each substring voltage is 12 V for V_{String} to be 36 V under practical conditions). The switch's duty cycle was manually swept to obtain efficiency characteristics.

The measured power conversion efficiencies are shown in Fig. 14(b). The prototype operated in DCM in the light-load region of output power lower than approximately 10 W, as designated with filled markers. For the greater output power region, the operations were in CCM and measured efficiencies exceeded 87%.

B. Experimental Equalizations

Experimental equalization tests were performed using Solar Array Simulators (E4350B, Agilent Technology) to emulate two cases of partially-shaded conditions: Cases 1 and 2 showed severely- and slightly-shaded conditions, corresponding to heavy- and light-load conditions, respectively, for ordinary converters. Inductor currents i_{L1}–i_{L3} were measured using current sensors to implement the optimum equalization strategy with I_{ref} = 50 mA.

Individual PV characteristics used for the first case, Case 1, are shown in Fig. 15; PV_1 and PV_2 are severely and moderately shaded, respectively, while PV_3 is unshaded. The theoretical extractable maximum power in Case 1—if all the substrings could ideally operate at each MPP— was 62.6 W. The string characteristic was swept using an electronic load, while I_{eq-i} (= I_{Li}), I_{String}, and I_{Load} were individually measured. The measured individual PV characteristics with equalization are shown in Figs. 16(a)–(c), in which I_{eq-i}, I_{String}, and I_{Load} are drawn as a function of V_{PVi}. The voltage equalizer in this case operated in CCM over the entire range. The shaded substrings, PV_1 and PV_2, received substantial equalization currents, I_{eq1} and I_{eq2}, of approximately 2 and 1 A, respectively, while that for the unshaded substring of PV_3, I_{eq3}, was controlled to be 50

(a) Experimental setup for efficiency measurement.

(b) Measured efficiencies.

Fig. 14.   (a) Experimental setup for efficiency measurement and (b) measured power conversion efficiencies.
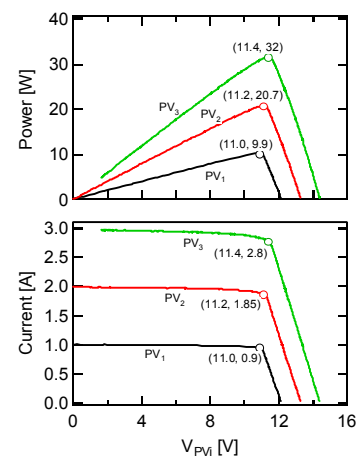

Fig. 15. Individual PV characteristics used for experimental equalization Case 1.
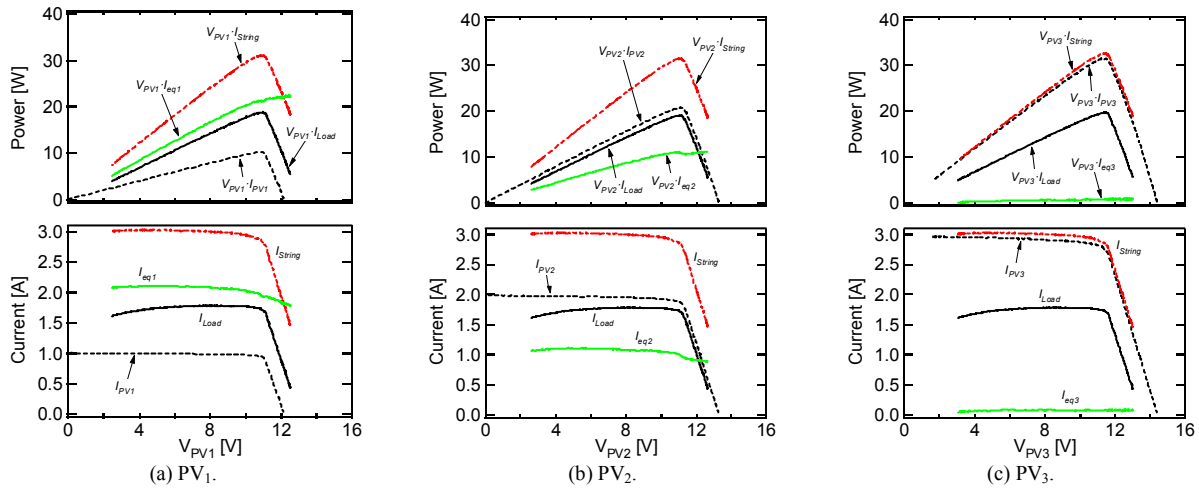
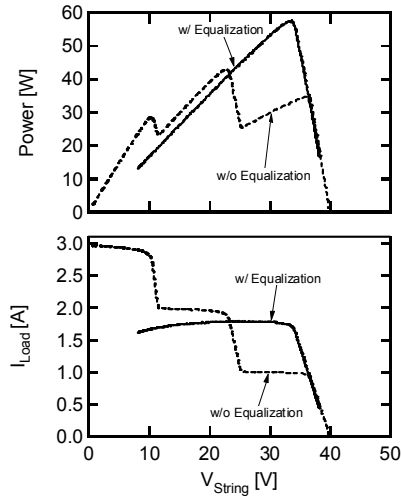Fig. 16. Measured individual PV characteristics with equalization in Case 1.

Fig. 17. String characteristics with and without equalization in Case 1.

Fig. 18. Measured key operation waveforms at V_{String} = 33 V in Case 1.

Fig. 19. Individual PV characteristics used for experimental equalization Case 2.

mA—all these currents obey (1). The measured I_{String}, which is the sum of I_{PVi} and I_{eq-i}, exceeded I_{Load}, and this difference corresponds to the input current of the equalizer, I_{eq-in}, as mentioned in Section II-B. All measured I_{Load}–V_{PVi} (or I_{String}–V_{PVi}) characteristics were nearly identical, demonstrating that all substring characteristics virtually become uniform with the support of the proposed voltage equalizer.

The measured characteristics of the PV string as a whole, with and without equalization, are shown and compared in Fig. 17. Without the voltage equalizer, three power point maxima, including two local and one global MPPs, were observed, and the extractable maximum power was approximately 42 W at V_{String} = 22 V. With the equalization, conversely, local MPPs successfully disappeared and the extractable maximum power increased to as much as 57.5 W at V_{String} = 33 V, at which the processed power and estimated power conversion loss in the equalizer were approximately 32.8 and 4.9 W, respectively. This result represents that 91.6% of the theoretical string power was extractable in Case 1. The unextractable string power is mainly attributable to the relatively large power conversion loss in the equalizer.
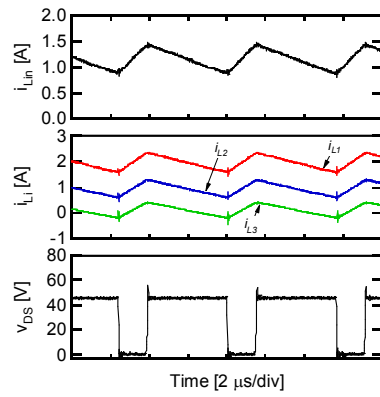
The measured key operational waveforms at V_{String} = 33 V are shown in Fig. 18. Inductor current ripples were the same for all of i_{Li}, whereas the average of i_{Li}, I_{Li}, was proportional to the degree of shading of respective substrings, as I_{Li} equates to I_{eq-i} (see (2)).

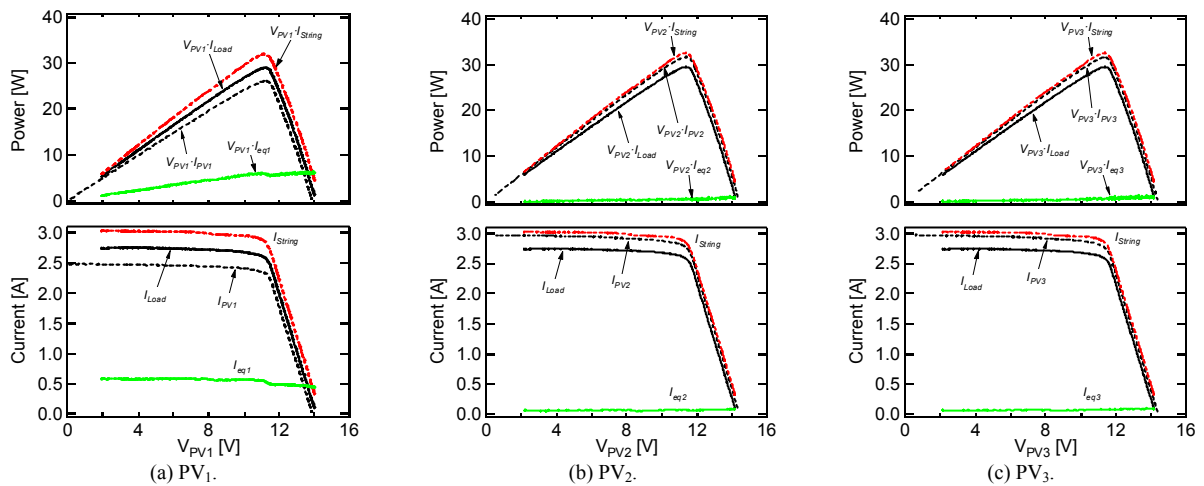The next experimental equalization test, Case 2, was

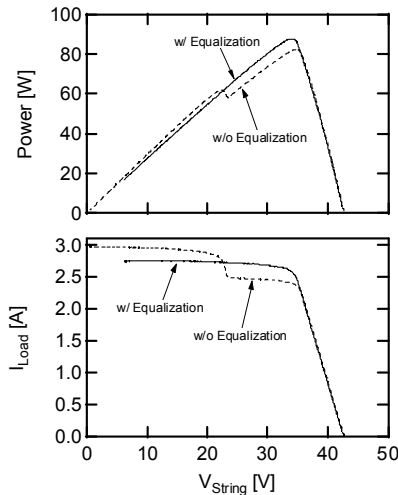Fig. 20. Measured individual PV characteristics with equalization in Case 2.

Fig. 21. String characteristics with and without equalization in Case 2.

Fig. 22. Measured key operation waveforms at V_{String} = 33 V in Case 2.

performed emulating the partially-shaded condition that only PV_1 is slightly shaded. The individual PV characteristics for Case 2 are shown in Fig. 19, and the theoretical extractable maximum power was 90 W. The measured individual PV characteristics in Case 2 are shown in Figs. 20(a)–(c). The equalizer operated in DCM because the degree of shading in Case 2 was light and corresponds to a light-load condition for ordinary converters, as mentioned in Section IV. Similar to Case 1, the shaded substring of PV_1 received substantial equalization current of I_{eq1}. Meanwhile both I_{eq2} and I_{eq3}, equalization currents for unshaded substrings of PV_2 and PV_3, were limited to 50 mA. All substrings exhibited virtually identical I_{Load}–V_{PVi} (or I_{String}–V_{PVi}) characteristics, even when the equalizer operated in DCM.

The measured string characteristics with and without equalization are compared in Fig. 21. Although the improvement in Case 2 was not as significant as that in Case 1, the local MPP found in the case without equalization was eliminated and the extractable maximum power was increased from 82.4 to 87.9 W by the voltage equalizer. The processed power and power conversion loss at the string's MPP were
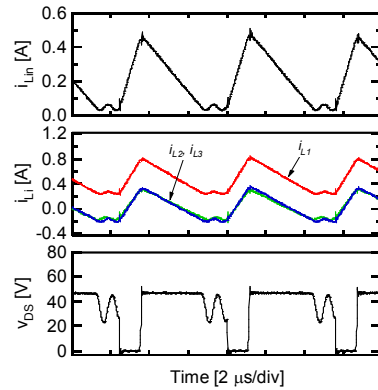
approximately 7.3 and 1.1 W, respective. Although the measured power conversion efficiencies were about 87% (Fig. 14(b)) and individual MPPT was unfeasible with the proposed voltage equalizer, 97.7% of the theoretical string power was extractable with the proposed equalizer in Case 2. This value is superior to that in Case 1 mainly because of the reduced power conversion loss as well as the processed power—the degree of characteristic mismatch in Case 2 was rather slight compared to that in Case 1.

The measured key waveforms at V_{String} = 33 V are shown in Fig. 22. The measured current waveforms were discontinuous triangular waves, while oscillations caused by the parasitic output capacitance of the MOSFET switch were observed. i_{L1} exceeded the others and its average was substantial, as only PV_1 was shaded in Case 2.

VII. CONCLUSIONS

Single-switch voltage equalizers for partially-shaded PV modules have been proposed in this paper. The proposed voltage equalizers can be derived by stacking CLD filters on traditional buck-boost converters, such as SEPIC, Zeta, and Ćuk converters. The single switch topology can simplify the circuitry compared with conventional DPP converters and voltage equalizers requiring numerous switches proportional to the

number of PV substrings/modules in series.

Depending on the equalization strategies, the proposed voltage equalizers might supply excessive equalization currents for unshaded substrings, needlessly increasing power conversion loss. The optimum equalization strategy, with which equalization currents for unshaded substrings are minimized, was proposed and discussed for the equalizers to work efficiently. Operational analyses based on the simplified equivalent circuit were also performed for the SEPIC-based equalizer, and a control circuit that substantiates the optimum equalization strategy was also introduced.

Experimental equalization tests emulating partial-shading conditions for a PV panel consisting of three substrings were performed using the prototype, and measured string characteristics with and without equalization were compared. Each PV substring received an equalization current from the equalizer depending on its degree of shading, and all substrings exhibited virtually uniform characteristics. Local MPPs found in the case without equalization were successfully eliminated by the support of the equalizer. The extractable maximum powers with equalization were considerably increased compared with those without equalization, demonstrating the efficacy of the proposed voltage equalizer.

REFERENCES

[1] S. Poshtkouhi, V. Palaniappan, M. Fard, and O. Trescases, "A general approach for quantifying the benefit of distributed power electronics for fine grained MPPT in photovoltaic applications using 3-D modeling," *IEEE Trans. Power Electron.*, vol. 27, no. 11, pp. 4656–4666, Nov. 2012.

[2] M. Balato and M. Vitelli, "A hybrid MPPT techniques based on the fast estimate of the maximum power voltages in PV applications," *Int. Conf. Expo. Ecological Vehicles and Renewable Energies*, pp. 1–7, 2013.

[3] M. Balato and M. Vitelli, "A new strategy for the identification of the optimal operating points in PV applications with distributed MPPT," *Int. Conf. Expo. Ecological Vehicles and Renewable Energies*, pp. 1–6, 2013.

[4] M. Vitelli, " On the necessity of joint adoption of both distributed maximum power point tracking and central maximum power point tracking in PV systems," *Prog. Photovolt. Res. Appl.*, vol. 22, pp. 283-299, 2014.

[5] P. S. Shenoy, K. A. Kim, B. B. Johnson, and P. T. Krein, "Differential power processing for increased energy production and reliability of photovoltaic systems," *IEEE Trans. Ind. Power Electron.*, vol. 28, no. 6, pp. 2968–2979, Jun. 2013.

[6] H. J. Bergveld, D. Büthker, C. Castello, T. Doorn, A. D. Jong, R. V. Otten, and K. D. Waal, "Module-level dc/dc conversion for photovoltaic systems: the delta-conversion concept," *IEEE Trans. Power Electron.*, vol. 28, no. 4, pp. 2005–2013, Apr. 2013.

[7] S. Qin and R. C. N. P. Podgurski, "Sub-module differential power processing for photovoltaic applications," *IEEE Applied Power Electron. Conf. Expo.*, pp. 101–108, 2013.

[8] S. Qin, S. T. Cady, A. D. D. García, and R. C. N. P. Podgurski, "A distributed approach to MPPT for PV sub-module differential power processing," *IEEE Energy Conversion Conf. Expo.*, pp. 2778–2785, 2013.

[9] R. Kadri, J. P. Gaubert, and G. Champenois, "New converter topology to improve performance of photovoltaic power generation system under shading conditions," *Int. Conf. Power Eng. Energy Electrical Drives*, pp. 1–7, 2011.

[10] R. Kadri, J. P. Gaubert, and G. Champenois, "Centralized MPPT with string current diverter for solving the series connection problem in photovoltaic power generation system," *Int. Conf. Power Eng. Energy Electrical Drives*, pp. 116–123, 2011.

[11] R. Giral, C. A. R. Paja, D. Gonzalez, J. Calvente, À. C. Pastpr, and L. M. Salamero, "Minimizing the effects of shadowing in a PV module by means of active voltage sharing," *IEEE Int. Conf. Ind. Technol*, pp. 943–948, 2010.

[12] R. Giral, C. E. Carrejo, M. Vermeersh, A. J. Saavedra-Montes, and C. A. Ramos-Paja, "PV field distributed maximum power point tracking by means of an active bypass converter," *Int. Conf. Clean Electrical Power*, pp. 94–98, 2011.

[13] L. F. L. Villa, T. P. Ho, J. C. Crebier, and B. Raison, "A power electronics equalizer application for partially shaded photovoltaic modules," *IEEE Trans. Ind. Electron.*, vol. 60, no. 3, pp. 1179–1190, Mar. 2013.

[14] L. F. L. Villa, X. Pichon, F. S. Ardelibi, B. Raison, J. C. Crebier, and A. Labonne, "Toward the design of control algorithms for a photovoltaic equalizer: choosing the optimum switching strategy and the duty cycle," *IEEE Trans. Power Electron.*, vol. 29, no. 3, pp. 1447–1460, Mar. 2014.

[15] Z. Salam and M. Z. Ramli, "A simple circuit to improve the power yield of PV array during partial shading," *IEEE Energy Conversion Cong. Expo.*, pp. 1622–1626, 2012.

[16] T. Shimizu, O, Hashimoto, and G. Kimura, "A novel high-performance utility-interactive photovoltaic inverter system," *IEEE Trans. Power Electron.*, vol. 18, no. 2, pp. 704–711, Mar. 2003.

[17] T. Shimizu, M. Hirakata, T. Kamezawa, and H. Watanabe, "Generation control circuit for photovoltaic modules," *IEEE Trans. Power Electron.*, vol. 16, no. 3, pp. 293–300, May 2001.

[18] J. T. Stauth, M. D. Seeman, and K. Kesarwani, "Resonant switched-capacitor converters for sub-module distributed photovoltaic power namagement," *IEEE Trans. Power Electron.*, vol. 28, no. 3, pp. 1189–1198, Mar. 2013.

[19] S. B. Yaakov, A. Blumenfeld, A. Cervera, and M. Evzelman, "Design and evaluation of a modular resonant switched capacitor equalizer for PV panels," *IEEE Energy Conversion Cong. Expo.*, pp. 4129–4136, 2012.

[20] Y. Nimni and D. Shmilovitz, "Returned energy architecture for improved photovoltaic systems efficiency," *IEEE Int. Symp. Circuit Syst.*, pp. 2191–2194, 2010.

[21] C. Olalla, M. Rodríguez, D. Clement, J. Wang, and D. Makisimović, "Architecture and control of PV modules with submodule integrated converter," *IEEE Control and Modeling for Power Electron.*, pp. 1–6, 2012.

[22] C. Olalla, D. Clement, M. Rodríguez, and D. Makisimović, "Architectures and control of submodule integrated dc-dc converters for photovoltaic applications," *IEEE Trans. Power Electron.*, vol. 28, no. 6, pp. 2980–2997, Jun. 2013.

[23] C. Olalla, C. Deline, D. Clement, Y. Levron, M. Rodríguez, and D. Makisimović, "Performance of power limited differential power processing architectures in mismatched PV systems," *IEEE Trans. Power Electron.*, to be published.

[24] Q. Zhang, X. Sun, Y. Zhong, and M. Matui, "A novel topology for solving the partial shading problem in photovoltaic power generation system," *IEEE Power Electron. Motion Cont. Conf.*, pp. 2130–2135, 2009.

[25] J. Du, R. Xu, X. Chen, Y. Li, and J. Wu, "A novel solar panel optimizer with self-compensation for partial shadow condition," *IEEE Applied Power Electron. Conf. Expo.*, pp. 92–96, 2013.

[26] K. Nishijima, H. Sakamoto, and K. Harada, "A PWM controlled simple and high performance battery balancing system," in Proc. *IEEE Power Electron. Spec. Conf.*, Jun. 2000, pp. 517–520.

[27] P. A. Cassani and S. S. Williamson, "Feasibility analysis of a novel cell equalizer topology for plug-in hybrid electric vehicle energy-storage systems," *IEEE Trans. Veh. Technol.*, vol. 58, no. 8, Oct. 2009, pp. 3938–3946.

[28] P. A. Cassani and S. S. Williamson, "Design, testing, and validation of a simplified control scheme for a novel plug-ion hybrid electric vehicle battery cell equalizer," *IEEE Trans. Ind. Electron.*, vol. 57, no. 12, Dec. 2010, pp. 3956–3962.

[29] J. W. Kimball, B. T. Kuhn, and P. T. Krein, "Increased performance of battery packs by active equalization," in Proc. *IEEE Veh. Power Propulsion Conf.*, Sep. 2007, pp. 323–327.

[30] A. Baughman and M. Ferdowsi, "Double-tiered switched-capacitor battery charge equalization technique," *IEEE Trans. Ind. Appl.*, vol. 55, no. 6, Jun. 2008, pp. 2277–2285.

[31] M. Uno and K. Tanaka, "Influence of high-frequency charge-discharge cycling induced by cell voltage equalizers on the life performance of

lithium-ion cells," *IEEE Trans. Veh. Technol.*, vol. 60, no. 4, May 2011, pp. 1505–1515.

[32] Y. Yuanmao, K. W. E. Cheng, and Y. P. B. Yeung, "Zero-current switching switched-capacitor zero-voltage-gap automatic equalization system for series battery string," *IEEE Trans. Power Electron.*, vol. 27, no. 7, Jul. 2012, pp. 3234–3242.

[33] N. H. Kutkut, D. M. Divan, and D. W. Novotny, "Charge equalization for series connected battery strings," *IEEE Trans. Ind. Appl.*, vol. 31, no. 3, May/Jun. 1995, pp. 562–568.

[34] N. H. Kutkut, H. L. N. Wiegman, D. M. Divan, and D. W. Novotny, "Charge equalization for an electric vehicle battery system," *IEEE Trans. Aerosp. Electron. Syst.*, vol. 34, no. 1, Jan. 1998, pp. 235–246.

[35] N. H. Kutkut, H. L. N. Wiegman, D. M. Divan, and D. W. Novotny, "Design considerations for charge equalization of an electric vehicle battery system," *IEEE Trans. Ind. Appl.*, vol. 35, no. 1, Jan. 1999, pp. 28–35.

[36] J. Cao, N. Schofield, and A. Emadi, "Battery balancing methods: a comprehensive review," in Proc. *IEEE Veh. Power Propulsion Conf.*, Sep. 2008, pp. 1–6.

[37] K. Z. Guo, Z. C. Bo, L. R. Gui, and C. S. Kang, "Comparison and evaluation of charge equalization technique for series connected batteries," in Proc. *IEEE Power Electron. Spec. Conf.*, Jun. 2006, pp. 1–6.

[38] M. Uno and K. Tanaka, "Single-switch cell voltage equalizer using multistacked buck–boost converters operating in discontinuous conduction mode for series-connected energy storage cells," *IEEE Trans. Veh. Technol.*, vol. 60, no. 8, Oct. 2011, pp. 3635–3645.

[39] V. Eng and C. Bunlaksananusorn, "Modeling of a SEPIC converter operating in continuous conduction mode," in Proc. *6th ECTI-CON*, pp. 136–139, May 2009.

[40] V. Eng and C. Bunlaksananusorn, "Modeling of a SEPIC converter operating in discontinuous conduction mode," in Proc. *6th ECTI-CON*, pp. 140–143, May 2009.

[41] D. S. L. Simonetti, J. Sebastián and J. Uceda, "The discontinuous conduction mode Sepic and Ćuk power factor preregulators: analysis and design," *IEEE Trans. Ind. Electron.*, vol. 44, no. 5, pp. 630–637, Oct. 1997.

Masatoshi Uno (M'06) was born in Japan in 1979. He received the B.E. degree in electronics engineering and the M.E. degree in electrical engineering from Doshisha University, Kyoto, Japan, in 2002 and 2004, respectively, and the Ph.D degree from the Graduate University for Advanced Studies, Kanagawa, Japan, in 2012.

Since 2004, he has been with Japan Aerospace Exploration Agency where he is currently a development researcher for spacecraft power systems. His research areas include switching power converters, cell equalizers, and life evaluation for supercapacitors and lithium-ion batteries, and development of fuel cell systems, for spacecraft power systems.

M. Uno is a member of the Institute of Electrical Engineering of Japan (IEEJ), and the Institute of Electronics, Information and Communication Engineers (IEICE).

Akio Kukita was born in Japan in 1967. He received the B.E. degree in physics from Chuo University, Japan, in 1993.

From 1993 to 1996 and 1996 to 2008, he was with SEIKO Holdings Corporation and Ebara Corporation, respectively. Since 2008, he has been with Japan Aerospace Exploration Agency as a senior engineer. His recent work has focused on the development of spacecraft power systems.